STEADY ANALYSIS OF THREE SURFACE AIRPLANES: IMPROVING THE AERODYNAMIC PERFORMANCE THROUGH REDUNDANT LONGITUDINAL CONTROL.

Stefano Cacciola[1], Carlo E D Riboldi[1] & Carlo Spitale[1]

[1]Department of Aerospace Science and Technology, Politecnico di Milano, Via La Masa 34, 20156 Milano, Italy.

Abstract

In the attempt to make aviation more energy efficient, both academia and industry are seeking innovative propulsion systems, improved aerodynamic designs, or unusual configurations. However, smart usage of existing configurations can play a prominent role in this context. In this work, we exploit the possibility of increasing the lift-to-drag ratio of a complete aircraft, using a three-surface configuration with redundant longitudinal control, obtained through two movable surfaces located respectively on the horizontal tail and canard. In a nutshell, the idea is exploiting the redundancy to minimize the drag of the entire airplane at each wind speed (and hence each lift coefficient). The numerical analysis performed in this work shows that a standard back-tailed airplane can be updated by adding a third surface, equipped with a degree of control, leading a similar aircraft with an improved lift-to-drag ratio.

Keywords:

1. Introduction

Airplane configurations based on three-lifting surfaces have been widely considered among aeronautical aircraft designers as a possible alternative to conventional back-tailed planes. Throughout history, such a configuration has always been proposed as an efficient solution, as witnessed by P180 experience [1], and by literature that has shown its potential advantages as a means for improving trim [2, 3] and suppressing flutter in highly flexible aircraft [4].

However, this design has never gained the upper hand over traditional two-surface configurations.

A reason for that probably lies in the intrinsic complexity of aerodynamics, which is characterized by the mutual interaction between multiple surfaces [5]. It is expected that the deflection of the flow induced by the upstream surfaces will impact the performance of the downstream ones: the tail feels the flow deflected by the wing, which, on its own, feels a flow deflected by the canard. However, if the canard and the wing are close, as typically happens in three-surface configurations, the upwash in front of the wing may also affect the flow at canard location, a phenomenon usually neglected in traditional airplanes.

Recently, a redundant longitudinal control has been studied in conjunction with the three-surface configuration, where both the canard and tail feature a movable part [6]. When these two controls are present, the longitudinal trim problem, consisting of finding the equilibrium in terms of the vertical forces and pitching moments, becomes overdetermined. The additional degree of freedom can then be used for optimization purposes, such as the minimization of overall drag. In Ref. [6] a detailed flight mechanics model of the three-surface airplane with redundant longitudinal control was introduced, extending standard lumped two-surface models (e.g. [7], chapter 3) by including the canard surface and a suitable modeling of the canard-wing interactions [8]. The preliminary results reported in [6] show that such redundancy is effective in minimizing the trim drag and in increasing the achievable maximum lift-to-drag-ratio of some percentage points.

Moreover, in [9], it was also possible to demonstrate that the redundancy in the longitudinal control may also be associated with improved take-off performance.
Notwithstanding the promising results, having a simple but accurate aerodynamic characterization of three-surface airplanes, featuring redundant longitudinal control, still represents an urgent need to allow a suitable preliminary design of such systems.
With the goal of further analyzing the performance of three-surface airplanes including redundant longitudinal control, in the present work, we extend the work of [6] in three directions:

1. First, we develop a Matlab tool for the estimation of the airplane aerodynamic model of a three-surface airplane based on the Digital Datcom software [10], in contrast with previous works where more simple models were employed.

2. We include in the trim optimization problem also the cancellation of the hinge moments of both control surfaces. This requires enlarging the array of the trim optimal variables with the incidence of both canard and tail, in addition to the angle of attack and the deflection of elevator and canard movable surfaces.

3. We formulate a preliminary design problem for three-surface airplanes aimed at finding some geometrical parameters related to wing, tail, and canard, to optimize the maximum lift-to-drag ratio of the trimmed polar.

In this paper, we will first show some features of the tool for the estimation of the aerodynamic model of the three-surface airplane. Then, we will detail the optimization of the trim including the cancelation of the hinge moments, exploiting the control redundancy. Finally, we will show the results of a design process aimed at updating a twin-engine propeller-driven airplane as an equivalent three-surface model featuring a higher lift-to-drag ratio.

2. Methodology

2.1 Using Datcom for modeling the aerodynamics of a three-surface airplane with redundant longitudinal control.

The purpose of this section is to describe a procedure for obtaining the stability and control derivatives and, more in general, the aerodynamic model of the three-surface airplane from the Digital Datcom Software. In this work, we focus on the steady aerodynamic models and, accordingly, on the steady constitutive equations for the lift coefficient C_L, drag coefficient C_D, pitch moment coefficient about the center of gravity C_{m_G} and hinge moment coefficients of the tail C_{H_T} and of the canard C_{H_C}. All these variables are defined as functions of five trim parameters, i.e. the angle of attack α, the deflection of the elevator δ_E, the deflection of the movable part of the canard δ_C and the incidence of tail i_T and canard i_C,

$$\begin{cases} C_L = & C_{L0} + C_{L\alpha}\alpha + C_{L\delta_\mathrm{E}}\delta_\mathrm{E} + C_{L\delta_\mathrm{C}}\delta_\mathrm{C} + C_{Li_\mathrm{T}}i_\mathrm{T} + C_{Li_\mathrm{C}}i_\mathrm{C} \\ C_{m_G} = & C_{m_G0} + C_{m_G\alpha}\alpha + C_{m_G\delta_\mathrm{E}}\delta_\mathrm{E} + C_{m_G\delta_\mathrm{C}}\delta_\mathrm{C} + C_{m_Gi_\mathrm{T}}i_\mathrm{T} + C_{m_Gi_\mathrm{C}}i_\mathrm{C} \\ C_{H_\mathrm{T}} = & C_{H_\mathrm{T}0} + C_{H_\mathrm{T}\alpha}\alpha + C_{H_\mathrm{T}\delta_\mathrm{E}}\delta_\mathrm{E} + C_{H_\mathrm{T}\delta_\mathrm{C}}\delta_\mathrm{C} + C_{H_\mathrm{T}i_\mathrm{T}}i_\mathrm{T} + C_{H_\mathrm{T}i_\mathrm{C}}i_\mathrm{C} \\ C_{H_\mathrm{C}} = & C_{H_\mathrm{C}0} + C_{H_\mathrm{C}\alpha}\alpha + C_{H_\mathrm{C}\delta_\mathrm{E}}\delta_\mathrm{E} + C_{H_\mathrm{C}\delta_\mathrm{C}}\delta_\mathrm{C} + C_{H_\mathrm{C}i_\mathrm{T}}i_\mathrm{T} + C_{H_\mathrm{C}i_\mathrm{C}}i_\mathrm{C} \end{cases} \tag{1}$$

where symbols $C_{\sigma 0}$ and $C_{\sigma\xi}$ represent the constant value of the generic coefficient C_σ, with $\sigma = (L, D, m_G, H_\mathrm{T}, H_\mathrm{C})$, and its derivative with respect to trim variable ξ. The drag coefficient, on the other hand, features a more complex and nonlinear behavior with respect to the trim variable, which can be formalized as

$$C_D = C_D(\alpha, \delta_\mathrm{E}, \delta_\mathrm{C}, i_\mathrm{T}, i_\mathrm{C}). \tag{2}$$

Equation (2) also assumes combined interactions among the angle of attack and the deflections of the control surfaces.
Estimating the entire model with a single run in Datcom is impossible as the compendium only considers canard or back-tailed configurations, hence airplanes featuring both lifting surfaces cannot be directly modeled. To cope with this, the estimation problem was split into multiple subproblems, exploiting and combining the analyses already available in Datcom.

A key aspect in this context is that Datcom also allows one to generate aerodynamic models of usual back-tailed airplanes where the wing is included through its aerodynamic derivatives already estimated with other methods. This possibility will be exploited for modeling three-surface airplanes as explained in the following paragraphs.

2.1.1 Estimation of lift and pitching moment coefficients

Starting from the constitutive equation for lift coefficient, i.e. the first of Eq. (1), the values of the parameters C_{L0}, $C_{L\alpha}$, $C_{L\delta_\mathrm{E}}$, $C_{L\delta_\mathrm{T}}$, C_{Li_T} and C_{Li_C} should be estimated for a given configuration.
To do so, four analyses are performed through Datcom. The first one considers the combination of the canard and the wing and generates a preliminary aerodynamic model of all aerodynamic bodies in front of the tail, including the derivative of the lift coefficient with respect to the deflection of the movable part of the canard δ_C, $C_{L_{\delta_C}}$. The second analysis, on the other hand, considers a back-tailed configuration with the physical tail and an artificial wing described through the aerodynamic model generated in the previous run. Hence, such an artificial wing incorporates the mutual interaction between the canard and the real wing. After the second one of this two-step analysis, we have access to the coefficients C_{L_α}, $C_{L_{\delta_E}}$ and C_{L_0} of the complete three-surface airplane. Notice that, within this approach, not only is the down-wash of the wing on the tail included but also the mutual interaction between canard and wing. On the other hand, any direct aerodynamic interference between the canard and the tail is neglected. This fact, however, is not considered critical because of the distance between the two surfaces.
Finally, the derivatives taken with respect to the incidences of tail and canard, $C_{L_{i_T}}$ and $C_{L_{i_C}}$, are estimated through two analyses, one for the canard alone and one for the tail alone. Obviously, for isolated surfaces, the incidence and the angle of attack correspond to the same degree of freedom. Consequently, indicating with ${C_{L\alpha}}^{(\mathrm{T})}$ and ${C_{L\alpha}}^{(\mathrm{C})}$, respectively, the derivative of the isolated tail and isolated canard with respect to the angle of attack, the desired derivatives are computed as

$$C_{L_{i_T}} = \eta_\mathrm{T}\,\sigma_\mathrm{T}\,{C_{L\alpha}}^{(\mathrm{T})} \tag{3}$$

and

$$C_{L_{i_C}} = \eta_\mathrm{C}\,\sigma_\mathrm{C}\,{C_{L\alpha}}^{(\mathrm{C})} \tag{4}$$

where σ_T is the ratio between the tail and the wing surfaces, σ_T is the ratio between canard and wing surface, whereas η_T and η_C are the ratio between the free-stream dynamic pressure and the dynamic pressure felt at the surface location, respectively for the tail and canard. Clearly, being the canard in the front of the airplane, η_C can be safely assumed equal to one.
Finally, all values of the dynamic pressure ratios result dependent on the angle of attack, to capture its impact on the wake of the upstream surface. Similarly, the estimated derivatives are typically dependent on the angle of attack, as a result of the intrinsic nonlinear nature of the aerodynamics.
Concerning the pitching moment constitutive law, as represented by the second equation of (1), the values of the coefficients C_{m_G0}, $C_{m_G\alpha}$, $C_{m_G\delta_\mathrm{E}}$, $C_{m_G\delta_\mathrm{C}}$, $C_{m_Gi_\mathrm{T}}$ and $C_{m_Gi_\mathrm{C}}$ of the three-surface airplane are to be determined.
The approach to estimate all these quantities is the same as already applied for the lift coefficient. In particular, C_{m_G0}, $C_{m_G\alpha}$, $C_{m_G\delta_\mathrm{E}}$, $C_{m_G\delta_\mathrm{C}}$ are extracted from the two-step analysis, while the derivatives with respect to the incidences i_T and i_C are obtained from the analyses of the isolated canard and horizontal tail. In particular, for the determination of the $C_{m_Gi_\mathrm{T}}$ coefficient, the analysis of the isolated horizontal tail is used for computing the tail-specific ${C_{m_G}}_\alpha^{(\mathrm{T})}$ coefficient. Notice that, even if this analysis considers an isolated surface, the pole about which the pitching moment is reduced coincides with the center of gravity of the overall airplane. Then, the airplane-specific coefficient is computed as

$$C_{m_Gi_\mathrm{T}} = \eta_\mathrm{T}\,\sigma_\mathrm{T}\,\kappa_\mathrm{T}\,{C_{m_G}}_\alpha^{(\mathrm{T})} \tag{5}$$

where κ_T is the ratio between the mean aerodynamic chords of the tail and that of the wing.
The same approach was used for computing the derivative with respect to the canard incidence, i_C, resulting in the relation

$$C_{m_Gi_\mathrm{C}} = \eta_\mathrm{C}\,\sigma_\mathrm{C}\,\kappa_\mathrm{C}\,{C_{m_G}}_\alpha^{(\mathrm{C})} \tag{6}$$

where $C_{m_G\alpha}^{(\mathrm{C})}$ is the canard-specific derivative and κ_C is the ratio between the mean aerodynamic chords of the canard and that of the wing.
Figure 1 schematically summarizes the process followed to estimate lift and pitching moment coefficients.

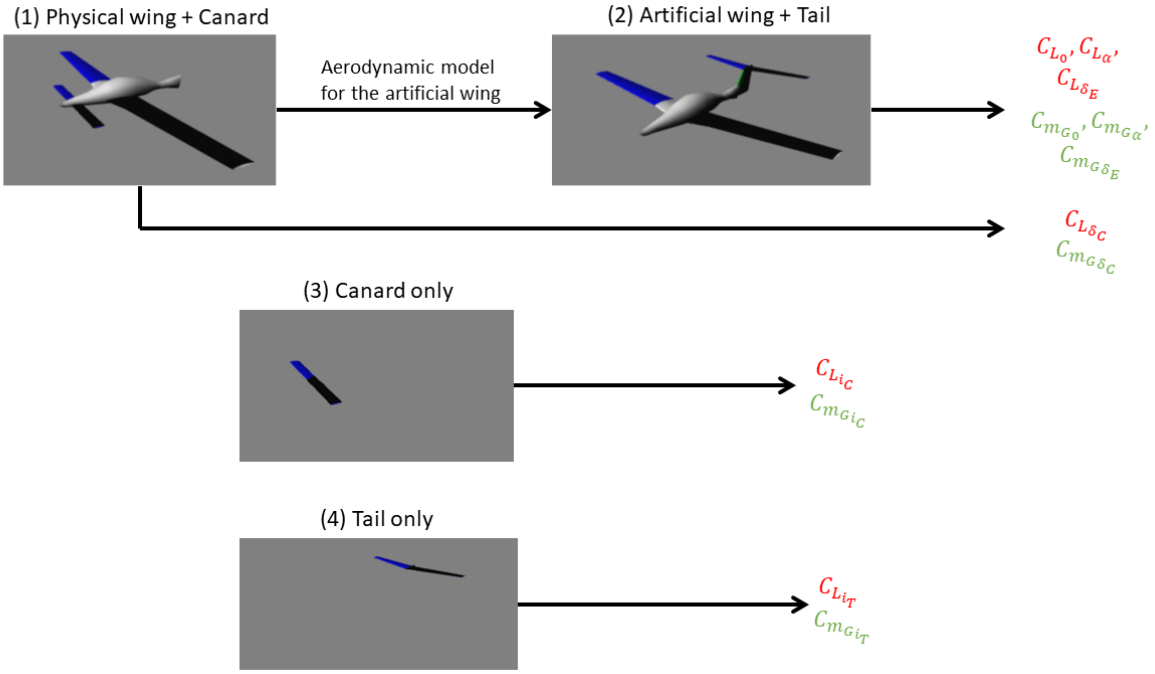

Figure 1 – Process to model lift and pitching moment coefficients in Datcom for three-surface airplanes.

2.2 Estimation of the hinge moment Coefficients

The problem of estimating the derivatives of the hinge moment of the elevator and canard movable part is simplified, assuming that each moment is linearly dependent on the variables associated with the surface on which the hinge is located. Moreover, constant coefficients, i.e. $C_{H_{\mathrm{T}0}}$ and $C_{H_{\mathrm{C}0}}$, were imposed equal to zero.
Therefore, the hinge moment coefficient of the horizontal tail depends solely on α, δ_E, and i^T, while that of the canard is a function of α, δ_C, and i_C. Given these considerations, it follows that

$$\begin{cases} C_{H_\mathrm{T}} = & C_{H_{\mathrm{T}\alpha}}\alpha + C_{H_{\mathrm{T}\delta_\mathrm{E}}}\delta_\mathrm{E} + C_{H_{\mathrm{T}i_\mathrm{T}}} i_\mathrm{T} \\ C_{H_\mathrm{C}} = & C_{H_{\mathrm{C}\alpha}}\alpha + C_{H_{\mathrm{C}\delta_\mathrm{C}}}\delta_\mathrm{C} + C_{H_{\mathrm{C}i_\mathrm{C}}} i_\mathrm{C} \end{cases} \tag{7}$$

The estimation of $C_{H_{\mathrm{T}\alpha}}$, $C_{H_{\mathrm{T}\delta_\mathrm{E}}}$, $C_{H_{\mathrm{C}\alpha}}$ and $C_{H_{\mathrm{C}\delta_\mathrm{C}}}$ are obtained from the two-step analysis of the complete aircraft. On the other side, the derivatives with respect to the incidence are computed from isolated tail and isolated canard analyses.
As mentioned earlier, for the isolated surfaces, the angle of attack can be interpreted as the incidence angle of that surface, hence the derivatives of the hinge moments with respect to the incidences equal the same derivatives respective to the angle of attack. Hence,

$$C_{H_{\mathrm{T}i_\mathrm{T}}} = C_{H_\mathrm{T}\alpha}^{(\mathrm{T})}, \tag{8}$$

and

$$C_{H_{\mathrm{C}i_\mathrm{C}}} = C_{H_\mathrm{C}\alpha}^{(\mathrm{C})}, \tag{9}$$

where $C_{H_\mathrm{T}\alpha}^{(\mathrm{T})}$ and $C_{H_\mathrm{C}\alpha}^{(\mathrm{C})}$ are the tail- and canard-specific moment derivatives with respect to the angle of attack, that are obtained from the analyses of the isolated surfaces.

2.3 Estimation of drag coefficient constitutive law

Despite the models for lift and pitching moment coefficients are typically linear in the aerodynamic parameters and are considered adequate to predict the aerodynamic performance of a generic aircraft, at least before stall, when it comes to defining the constitutive law of the drag, one has to consider generic nonlinear functions.

For this reason, it is necessary to define a suitable model structure to capture the variation of the drag with the angle of attack α and the deflection of the control surface δ_E and δ_C. To do so, we were inspired by the way Datcom models the drag coefficients, through the sum of three contributions: an angle-of-attack-dependent coefficient $C_D(\alpha)$, a variation in parasite drag coefficient $\Delta C_{D_0}(\delta)$ attributed to longitudinal control deflection δ, and a variation in induced drag coefficient $\Delta C_{D_i}(\alpha,\delta)$ function of both α and δ. Consequently, the generic drag function reads

$$C_D(\alpha,\delta) = C_D(\alpha) + \Delta C_{D_0}(\delta) + \Delta C_{D_i}(\alpha,\delta). \tag{10}$$

Following the same idea, we can model the drag of three surface airplane by including, along with the angle-of-attack-dependent coefficient $C_D(\alpha)$, three contributions related to the four control variables, $\Delta C_{D_0}(\delta_E)$, $\Delta C_{D_0}(\delta_C)$ $\Delta C_{D_0}(i_\mathrm{T})$ and $\Delta C_{D_0}(i_\mathrm{C})$, and other four contributions to the induced drag dependent on the combinations of the angle of attack and the control variables, $\Delta C_{D_i}(\alpha,\delta_E)$, $\Delta C_{D_i}(\alpha,\delta_C)$, $\Delta C_{D_i}(i_\mathrm{T},\delta_E)$ and $\Delta C_{D_i}(i_\mathrm{C},\delta_C)$.

The final drag equation for the three-surface airplane $C_D^{(3S)}(\alpha,\delta_E,\delta_C,i_\mathrm{T},i_\mathrm{C})$ results

$$\begin{aligned} C_D^{(3S)}(\alpha,\delta_E,\delta_C,i_\mathrm{T},i_\mathrm{C}) = \quad & C_D(\alpha) + \Delta C_{D_0}(\delta_E) + \Delta C_{D_0}(\delta_C) + \Delta C_{D_0}(i_\mathrm{T}) + \Delta C_{D_0}(i_\mathrm{C}) + \\ & + \Delta C_{D_i}(\alpha,\delta_E) + \Delta C_{D_i}(\alpha,\delta_C) + \Delta C_{D_i}(i_\mathrm{T},\delta_E) + \Delta C_{D_i}(i_\mathrm{C},\delta_C). \end{aligned} \tag{11}$$

Notice that, in this equation, additional terms related to possible couplings between the tail and canard were not considered. Because of the distance between these two surfaces, this is expected to be a good assumption.

To estimate all these parameters, it is possible to exploit the same analyses employed for the estimation of the lift and pitching moment coefficients described in Sec. 2.1.1.

In particular from the two-step analysis, i.e. steps (1) and (2) in Fig. 1, one estimates a drag, indicated here with the superscript (TS), associated with the three surface airplane with the sole elevator as the control surface. This model takes the form of

$$C_D^{(\mathrm{TS})} = C_D^{(\mathrm{TS})}(\alpha) + \Delta C_{D_0}{}^{(\mathrm{TS})}(\delta_E) + \Delta C_{D_i}{}^{(\mathrm{TS})}(\alpha,\delta_E) \tag{12}$$

and can be employed for estimating those coefficients of Eq. (11) that model the drag of the three-surface airplane and the mutual coupling between α and δ_E. Consequently,

$$C_D(\alpha) = C_D^{(\mathrm{TS})}(\alpha), \quad \Delta C_{D_0}(\delta_E) = \Delta C_{D_0}{}^{(\mathrm{TS})}(\delta_E), \quad \Delta C_{D_i}(\alpha,\delta_E) = \Delta C_{D_i}{}^{(\mathrm{TS})}(\alpha,\delta_E). \tag{13}$$

The contribution to the drag of the canard deflection δ_C and of the incidence of both tail and canard is not included and hence should be estimated through dedicated simulations.

To this end, from the two analyses of the isolated tail and the isolated canard, i.e. simulation (3) and (4) of Fig. 1, one estimates the model for the drag of the isolated tail, indicated with the superscript (T),

$$C_D^{(\mathrm{T})} = C_D^{(\mathrm{T})}(\alpha) + \Delta C_{D_0}{}^{(\mathrm{T})}(\delta_E) + \Delta C_{D_i}{}^{(\mathrm{T})}(\alpha,\delta_E), \tag{14}$$

and the model for isolated canard, indicated with the superscript (C)

$$C_D^{(\mathrm{C})} = C_D^{(\mathrm{C})}(\alpha) + \Delta C_{D_0}{}^{(\mathrm{C})}(\delta_C) + \Delta C_{D_i}{}^{(\mathrm{C})}(\alpha,\delta_C). \tag{15}$$

The tail- and canard-specific drag models provide for the remaining contributions needed to complete the drag model of the three-surface airplane in Eq. (11).

In fact, recalling that the change of the incidence corresponds to a physical change in the angle of attack, it is possible to recover the term $\Delta C_{D_i}(i_\mathrm{T},\delta_E)$ from $\Delta C_{D_i}{}^{(\mathrm{T})}(\alpha,\delta_E)$ as

$$\Delta C_{D_i}(i_\mathrm{T},\delta_E) = \eta_\mathrm{T}\,\sigma_\mathrm{T}\,\Delta C_{D_i}{}^{(\mathrm{T})}(\alpha,\delta_E), \tag{16}$$

and the term $\Delta C_{D_0}(i_\mathrm{T})$ from $C_D^{(\mathrm{T})}(\alpha)$ as

$$\Delta C_{D_0}(i_\mathrm{T}) = \eta_\mathrm{T}\,\sigma_\mathrm{T}\,C_D^{(\mathrm{T})}(\alpha), \tag{17}$$

Applying the same argument, also $\Delta C_{D_\mathrm{i}}(i_\mathrm{C},\delta_C)$ and $\Delta C_{D_0}(i_\mathrm{C})$ are computed from the terms $\Delta C_{D_\mathrm{i}}{}^{(\mathrm{C})}(\alpha,\delta_C)$ and $C_D^{(\mathrm{C})}(\alpha)$ as

$$\Delta C_{D_\mathrm{i}}(i_\mathrm{C},\delta_C) = \eta_\mathrm{C}\,\sigma_\mathrm{C}\,\Delta C_{D_\mathrm{i}}{}^{(\mathrm{C})}(\alpha,\delta_C) \tag{18}$$

and

$$\Delta C_{D_0}(i_\mathrm{T}) = \eta_\mathrm{C}\,\sigma_\mathrm{C}\,C_D^{(\mathrm{C})}(\alpha). \tag{19}$$

Finally, the variation in the parasite drag induced by the sole deflection of the canard control surface is computed out of the term $\Delta C_{D_0}{}^{(\mathrm{C})}(\delta_C)$ as

$$\Delta C_{D_0}(\delta_C) = \eta_\mathrm{C}\,\sigma_\mathrm{C}\,\Delta C_{D_0}{}^{(\mathrm{C})}(\delta_C) \tag{20}$$

while the induced contribution due to the coupling of α and δ_C is recovered from $\Delta C_{D_\mathrm{i}}{}^{(\mathrm{C})}(\alpha,\delta_C)$ as

$$\Delta C_{D_\mathrm{i}}(\alpha,\delta_C) = \eta_\mathrm{C}\,\sigma_\mathrm{C}\,\Delta C_{D_\mathrm{i}}{}^{(\mathrm{C})}(\alpha,\delta_C). \tag{21}$$

2.4 Optimization of trim including hinge moments.

The longitudinal trim of an airplane implies the satisfaction of the vertical equilibrium, of the pitching moments and the cancelation of the hinge moments. Given an aerodynamic model, the trim in horizontal flight conditions is formulated as

$$\begin{cases} C_L = & C_L^* = \frac{W}{qS} \\ C_{m_G} = & 0 \\ C_{H_\mathrm{T}} = & 0 \\ C_{H_\mathrm{C}} = & 0 \end{cases} \tag{22}$$

where C_L^* is the lift coefficient at trim, S the wing area, W the airplane weight and q the dynamic pressure. According to Eq. (1), C_L, C_{m_G}, C_{H_T} and C_{H_C} are expressed as functions of the five trim variables α, δ_E, δ_C, i_T and i_C. Equation (22) represents an undetermined linear system of four equations in five trim variables, that can be given a more compact form as

$$\boldsymbol{y} = \boldsymbol{X}\boldsymbol{\xi}, \tag{23}$$

where

$$\boldsymbol{y} = \begin{Bmatrix} C_L^* - C_{L0} \\ -c_{m_G 0} \\ -c_{H_\mathrm{T} 0} \\ -c_{H_\mathrm{C} 0} \end{Bmatrix}, \tag{24}$$

$$\xi = \{\alpha,\, \delta_E,\, \delta_C,\, i_\mathrm{T},\, i_\mathrm{C}\}^T, \tag{25}$$

and

$$\boldsymbol{X} = \begin{bmatrix} C_{L\alpha} & C_{L\delta_E} & C_{L\delta_C} & C_{Li_\mathrm{T}} & C_{Li_\mathrm{C}} \\ C_{m_G\alpha} & C_{m_G\delta_E} & C_{m_G\delta_C} & C_{m_Gi_\mathrm{T}} & C_{m_Gi_\mathrm{C}} \\ C_{H_\mathrm{T}\alpha} & C_{H_\mathrm{T}\delta_E} & C_{H_\mathrm{T}\delta_C} & C_{H_\mathrm{T}i_\mathrm{T}} & C_{H_\mathrm{T}i_\mathrm{C}} \\ C_{H_\mathrm{C}\alpha} & C_{H_\mathrm{C}\delta_E} & C_{H_\mathrm{C}\delta_C} & C_{H_\mathrm{C}i_\mathrm{T}} & C_{H_\mathrm{C}i_\mathrm{C}} \end{bmatrix}. \tag{26}$$

The indeterminacy of system (23) implies infinite parameter combinations solve the equilibrium and the cancelation of hinge moments. The idea, here, is that it is possible to exploit such an indeterminacy to optimize a particular merit function, i.e. to look for that parameter combination, among all satisfying Eq. (23), that results optimal from a desired point of view.

As it was already suggested in [6], a smart choice for solving the indeterminacy is to minimize the drag coefficient C_D of the overall airplane for a given lift coefficient $C_L^* = W/(qS)$.

The optimal trim problem can then be formalized as the following constrained optimization,

$$\boldsymbol{\xi}_{\text{trim}} = \arg\left(\min\left(C_D(\boldsymbol{\xi})\right)\right) \quad \text{s.t.} \quad \boldsymbol{y} = \boldsymbol{X}\boldsymbol{\xi} \tag{27}$$

that can be solved by standard optimization routines for any C_L and hence for any airplane speed, yielding the scheduling of the trim control variables as functions of the lift coefficient.
In [6], it was demonstrated that, if the drag model is quadratic in the parameters $\boldsymbol{\xi}$ and lift and moment coefficients are linear in $\boldsymbol{\xi}$, problem (27) can be solved in closed form and the trim variables assume the shape of straight lines with respect to C_L^*. In this work, however, we do not have the same assumptions; hence, the solution can only be found numerically.
Let us now consider that solution $\boldsymbol{\xi}_{\text{trim}}$ is a generic nonlinear function $\boldsymbol{f}$ of C_L^*, i.e. $W/(qS)$,

$$\boldsymbol{\xi}_{\text{trim}} = \boldsymbol{f}\left(C_L^*\right). \tag{28}$$

Equation (28) can be expanded by components, yielding the relationship between each optimal trim variable and the lift coefficient as

$$\begin{aligned} \alpha_{\text{opt}} &= f_{\alpha}\left(C_L^*\right) \\ \delta_{E\,\text{opt}} &= f_{\delta_E}\left(C_L^*\right) \\ \delta_{C\,\text{opt}} &= f_{\delta_C}\left(C_L^*\right) \\ i_{\text{T}\,\text{opt}} &= f_{i_{\text{T}}}\left(C_L^*\right) \\ i_{\text{C}\,\text{opt}} &= f_{i_{\text{C}}}\left(C_L^*\right) \end{aligned} \tag{29}$$

where f_{α}, f_{δ_E}, f_{δ_C}, $f_{i_{\text{T}}}$ and $f_{i_{\text{C}}}$ are the scalar nonlinear functions associated with each trim variable.
Finally, the optimal trimmed polar of the three-surface airplane can be computed by inserting Eq. (29) in Eq. (2) as

$$C_{D\text{opt}} = C_D(f_{\alpha}(C_L^*), f_{\delta_E}(C_L^*), f_{\delta_C}(C_L^*), f_{i_{\text{T}}}(C_L^*), f_{i_{\text{C}}}(C_L^*)) \tag{30}$$

From that polar, one can easily extract the optimal performance such as the maximum lift-to-drag ratio,

$$E_{\max} = \max\left(\frac{C_L^*}{C_{D\text{opt}}}\right), \tag{31}$$

and the maximum power index,

$$F_{\max} = \max\left(\frac{C_L^*\sqrt{C_L^*}}{C_{D\text{opt}}}\right), \tag{32}$$

associated respectively with the minimum required thrust and the minimum required power in steady horizontal flight (see [7], chapter 2).

2.5 Turning a standard two-surface airplane into a three-surface one with redundant longitudinal control through a design optimization

In order to evaluate if the three-surface configuration with redundant longitudinal control can be considered a valuable alternative to usual back-tailed configurations, a procedure to update an existing two-surface design is considered. The aim is to find a three-surface version of an existing airplane, that features a higher aerodynamic performance in terms of lift-to-drag ratio $E_{\max}$ and in terms of power index $E_{\max}$.

2.5.1 Definition of the equivalence between a two-surface and a three-surface airplane according to static margin and empennage volume

To have a fair comparison, the three-surface version and the nominal airplane must share some similar characteristics strongly connected with trim and controllability.
In this work, as similarly done in [6], we decided to create an equivalent three-surface airplane with unaltered wing, with the same static stability margin μ and the same empennage volume V_{emp}. The static margin, for both configurations, is defined conventionally, as

$$\mu = (x_G - x_N)/c, \tag{33}$$

where x_G and x_N are the longitudinal position of the center of gravity G and the neutral point N, whereas c is the mean aerodynamic chord of the wing. It is assumed that the longitudinal x-axis originates in the airplane nose and points forward. The location of the neutral point is defined as,

$$x_N = x_G + \frac{C_{m_{G\alpha}}}{C_{L\alpha}}. \tag{34}$$

Equation (34) is formally identical to the one used for conventional back-tailed airplanes. However, in the case of three-surface configurations, the derivative $C_{m_{G\alpha}}$ and $C_{L\alpha}$ also consider the presence of the third lifting surface.

Finally, the total empennage volume V_{emp} is defined as the sum of the tail volume V_{tail} and canard volume V_{canard}, computed as

$$V_{\text{tail}} = \frac{S_{\text{T}}\left(x_G - x_{AC_{\text{T}}}\right)}{Sc} \tag{35}$$

and

$$V_{\text{canard}} = \frac{S_{\text{C}}\left(x_{AC_{\text{C}}} - x_G\right)}{Sc}, \tag{36}$$

where $x_{AC_{\text{T}}}$ and $x_{AC_{\text{C}}}$ represent respectively the location of the aerodynamic centers of tail and canard surfaces. Obviously, in the case of traditional two-surface airplanes, V_{emp} corresponds to the sole tail volume V_{tail}.

The location of the center of gravity must also be updated to reflect the different configurations when passing from a reference two-surface to a modified three-surface airplane. To this end, the weight of both empennages W_{emp} is estimated through a semiempirical relationship, proposed in [11], that reads

$$W_{\text{emp}} = k_h S_{\text{emp}} \frac{3.81\, S_{\text{emp}} V_{\text{D}}}{1000\sqrt{\cos(\Lambda)}}, \tag{37}$$

where K_h is a coefficient whose value is 1 for fixed incidence and 1.1 for variable incidence stabilizers, S_{emp} is the empennage surface in ft^2, V_{D} is the dive speed in kn, λ is the sweep angle of the surface while resulting weight W_{emp} is given in lbf. Clearly, Eq. 37 can be employed to estimate the variation of both empennage weights and the implied change in the airplane center of gravity.

2.5.2 Optimization of the equivalent three-surface airplane

The constitutive laws of aerodynamic coefficients and hinge moments, expressed in Eqs. (1) and (2) with all parameters estimated through the process detailed in Secs. 2.1.1, 2.2 and 2.3, represent a parameterized steady flight mechanics model $\mathscr{M}(\boldsymbol{\theta})$, being $\boldsymbol{\theta}$ the array containing all design variables of the three-surface airplane. Model $\mathscr{M}(\boldsymbol{\theta})$ is also associated with an optimal drag polar obtained from the optimization process described in Sec. 2.4, that in turn features a specific maximum lift-to-drag ratio and maximum power index.

Within this context, by exploiting the aforementioned tools, the three-surface airplane design can be formulated as the problem of finding the design parameter array $\boldsymbol{\theta}_{\text{opt}}$ associated with the maximum lift-to-drag ratio and subjected to the constraint of having the same static margin and empennage volume of a reference two-surface airplane. Accordingly,

$$\boldsymbol{\theta}_{\text{opt}} = \arg\left(\max\left(E_{\max}\left(\boldsymbol{\theta}\right)\right)\right) \tag{38a}$$

$$\text{s.t.}$$

$$\mu(\boldsymbol{\theta}) = \mu_{\text{nom}} \tag{38b}$$

$$V_{\text{total}}(\boldsymbol{\theta}) = V_{\text{tail}_{\text{nom}}} \tag{38c}$$

where μ_{nom} and $V_{\text{tail}_{\text{nom}}}$ are respectively the static margin and the tail volume of the nominal, i.e. two-surface, airplane.

Notice also that in Eq. (38a), one could also choose to maximize the power index $F = (C_L\sqrt{C_L})/C_D$, yielding a possible different design solution.

Figure 2 summarizes the design process for the three-surface aircraft with redundant longitudinal control, consisting of two nested optimizations: the optimization of the trim that exploits the control

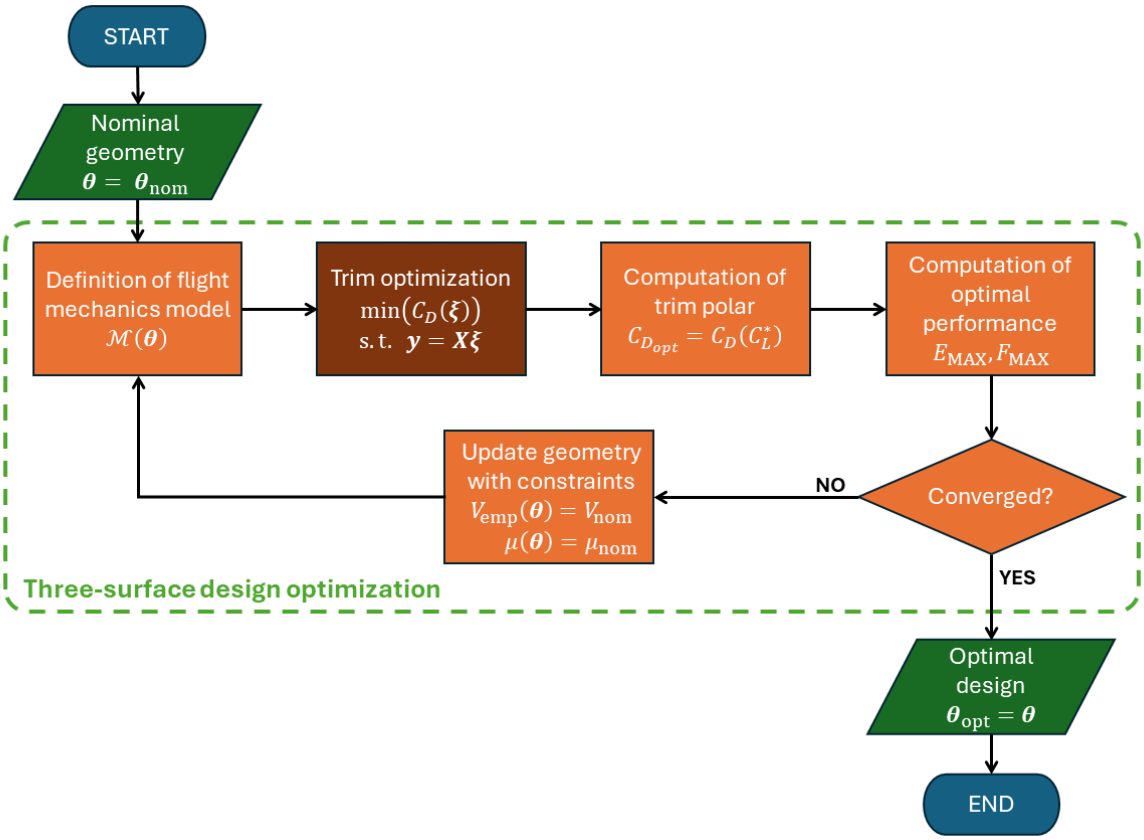

Figure 2 – Design process for the three-surface airplane with redundant longitudinal control, made by two nested optimizations: optimal trim definition exploiting the control redundancy (brown rectangle) and optimal design aimed at maximum lift-to-drag, or maximum power index (dashed light-green rectangle).

redundancy, reported in the brown rectangle, and the overall optimization aimed at maximizing the aerodynamic performance displayed within the dashed light green rectangle.
As a final remark, it is important to stress that, since problem (38) includes two equality constraints, the array $\boldsymbol{\theta}$ with the design parameters must be chosen in such a way the satisfaction of the constraints themselves is possible. This typically entails that the longitudinal location of the wing be an active optimization parameter.
In this work, the two nested constrained optimizations are performed by the SQP algorithm implemented in the Matlab function »`fmincon`, [12].

3. Results

In this section, we will discuss the initial results of updating a traditional two-surface airplane into a three-surface one featuring redundant longitudinal control, following the process detailed in Sec. 2. A similar exercise was already done in Ref. [6]. However, in that case, the formulation did not include hinge moments within the optimal trim definition and, additionally, the design was accomplished as a parametric study rather than through an optimization process.
At first, a flight mechanics model loosely based on the Diamond DA42 Twin Star was derived. The DA42 is a twin-engine propeller-driven airplane featuring a wing area of slightly more than $16\,\text{m}^2$ with a maximum take-off mass of $1900\,\text{kg}$.
The nominal model was subsequently updated into an equivalent three-surface airplane with redundant longitudinal control following the process of Sec. 2.5.
The longitudinal flight mechanics model of the nominal airplane was developed with the tool described in Secs. 2.1.1, 2.2and 2.3. Afterward, the trim equation was solved yielding the schedule of the control variables as a function of the lift coefficients.

The nominal airplane does not feature a redundant control, hence, the trim simply consists in the computation of the values of the angle of attack α, the deflection of the elevator δ_E, and the incidence of the tail i_C, that satisfy the vertical and pitching moment equilibrium and the cancelation of the tail hinge moment, i.e. the first, second and third lines of Eq. (22). Clearly, in this case, the trim problem considers three equations in three unknowns α, δ_E and i_C, and three equations, hence the problem is not overdetermined and does not allow one to optimize a desired merit figure.
Figure 3 shows the trim variables as functions of the lift coefficient C_L.

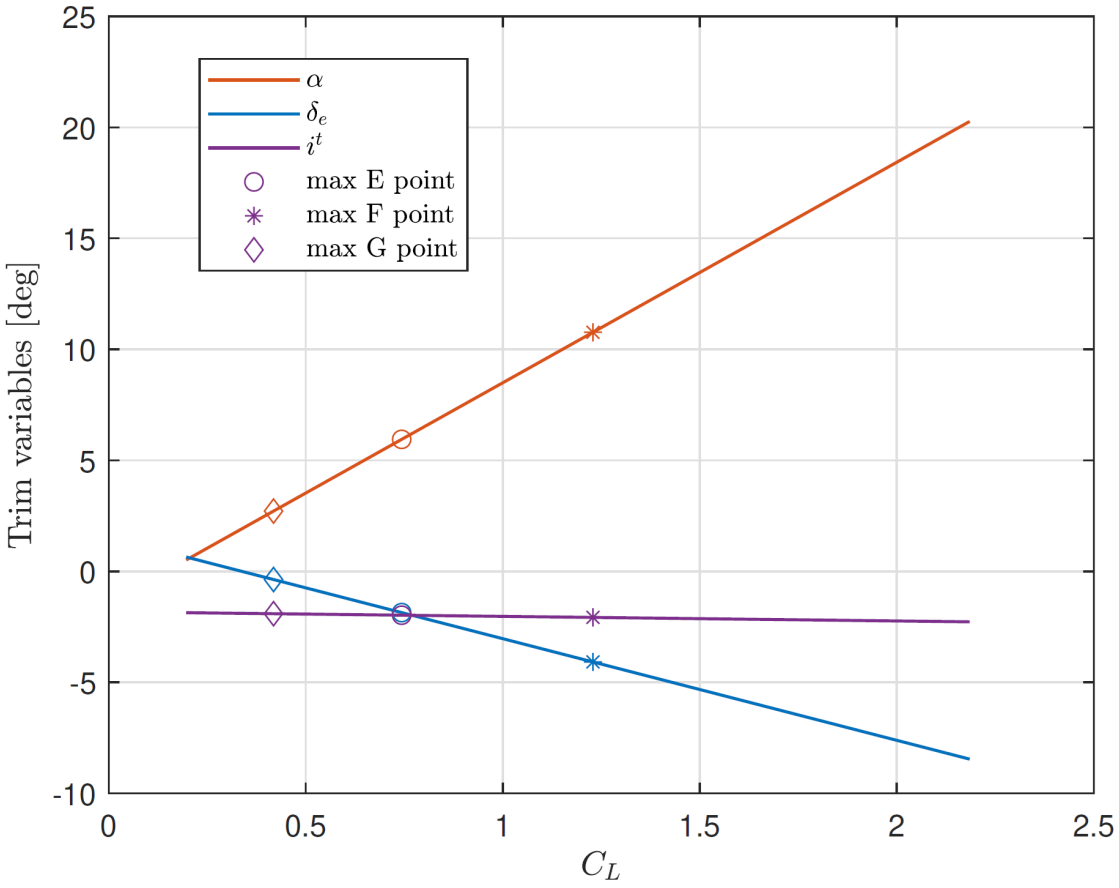

Figure 3 – Trim variable scheduling as a function of the lift coefficient for the nominal two-surface airplane

The plot also shows the points associated with the maximum lift-to-drag $E_{\max}$ (circle marker) and the maximum power index $F_{\max}$ (star marker). Additionally, the attitude that maximizes the index $G = \sqrt{C_L}/C_D$ is indicated with a diamond marker. Maximum G is associated with the maximum cruise range for jet airplanes and, therefore, is not interesting for the DA42. As expected, the trim angle of attack increases as C_L increases, while $delta_E$ decreases. The incidence, on the other hand, features a mild decrement as the lift coefficient increases, which is barely visible in the plot. The resulting maximum lift-to-drag ratio of the nominal airplane is equal to 20.
The nominal airplane was then updated as a three-surface airplane with redundant control using as optimization parameters the canard and tail surface S_C and S_T, the location of the aerodynamic center of the wing x_{AC_W}, that of the canard x_{AC_C}, and the aspect ratio of the canard λ_C. All these design variables are collected in vector $\boldsymbol{\theta} = \{S_C, S_T, x_{AC_W}, x_{AC_C}, \lambda_C\}^T$.
Two preliminary optimization tests were performed, changing the ratio between the elevator and the tail span, b_{elev}/b_{tail}.
In the first case, the elevator span ratio b_{elev}/b_{tail} was maintained equal to that of the nominal airplane $b_{elevnom}/b_{tailnom}$.
For this condition, Tab. 1 summarizes the optimal design parameters characterizing the equivalent three-surface airplane. Looking at the results, it is clear that the three-surface airplane features a

reduced tail as a consequence of the inclusion of the canard surface. To maintain the constraint related to the static margin, the wing moves $50\,\mathrm{cm}$ backward. The overall increase of the maximum lift-to-drag ratio is quite significant and can be quantified in about 33%.

Table 1 – Nominal airplane and optimized three-surface equivalent version.

	S_C m^2	$x_{\mathrm{AC_C}}$ m	$x_{\mathrm{AC_W}}$ m	λ_C	S_T m^2	E_max
Nominal	-	-	-2.21	-	2.35	20.04
Optimized	2.26	-0.0432	-2.89	3.55	1.34	26.64

Figure 4 shows the schedule of the trim variables as functions of the lift coefficients. The red curve refers to the angle of attack α, the blue and yellow ones respectively to elevator δ_E and canard δ_C deflections, whereas purple and green ones are respectively associated with tail i_T and canard i_C incidence. Dots indicate the point of maximum lift-to-drag ratio C_L/C_D (point E), the maximum power index $C_L\sqrt{C_L}/C_D$ (point F) and the maximum $\sqrt{C_L}/C_D$ (point G).

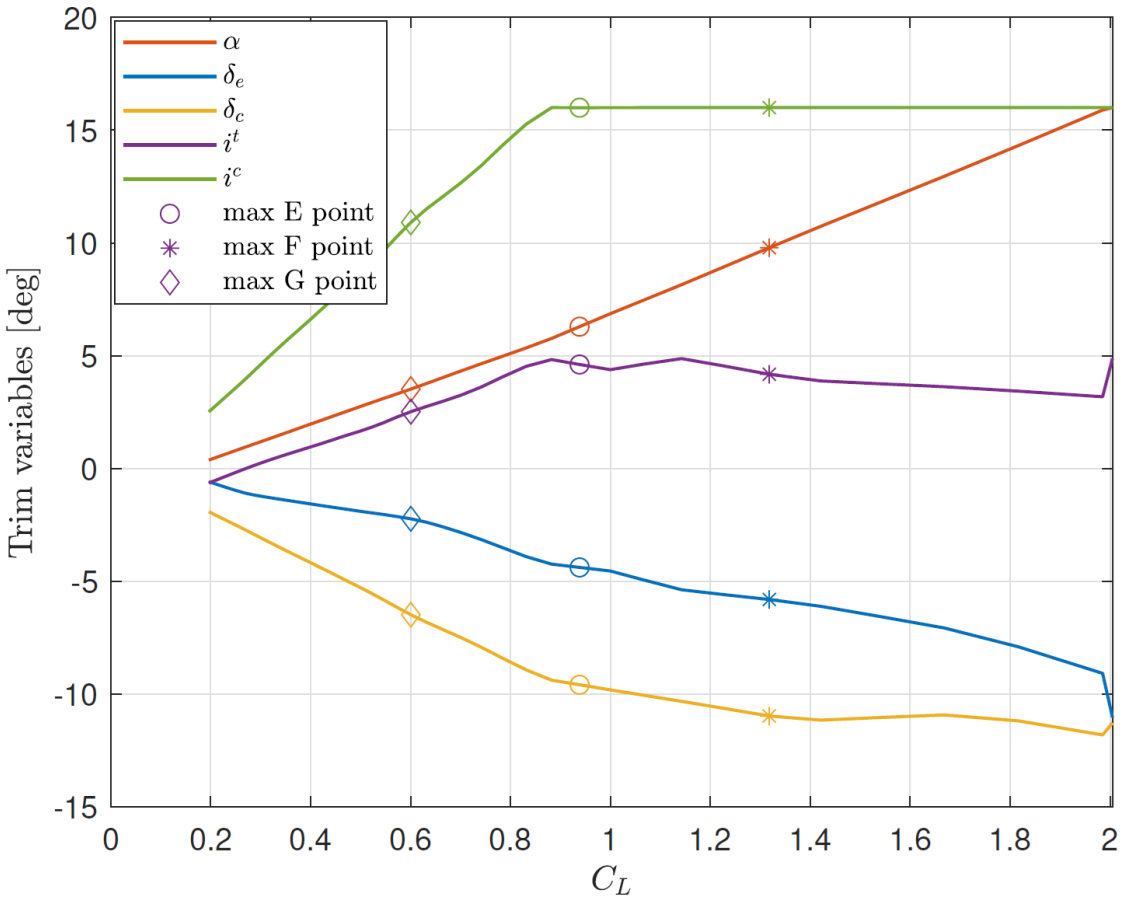

Figure 4 – Trim variable scheduling as a function of the lift coefficient for the equivalent three-surface airplane in the case of $b_\mathrm{elev}/b_\mathrm{tail} = b_\mathrm{elevnom}/b_\mathrm{tailnom}$

The behavior of the trim variables is nonlinear since the drag function is no longer quadratic. Moreover, at C_L equal to 0.9 the canard incidence hit the upper boundary of $16\,\mathrm{deg}$ causing the "knee" in the curves related to the incidence of canard and tail.
In a second test, the elevator span ratio was halved, i.e. $b_\mathrm{elev}/b_\mathrm{tail} = \frac{1}{2} b_\mathrm{elevnom}/b_\mathrm{tailnom}$. The obtained results are summarized in Tab. 2.
Also in this case, the maximum lift-to-drag ratio increased significantly from about 20 to 25.5 (27%) and similar conclusions with respect to the previous case can be derived. In particular, the optimal three-surface version of DA42 features a canard with surface $S_C = 2.23\,\mathrm{m}^2$, tail surface $S_\mathrm{T} = 1.35\,\mathrm{m}^2$

Table 2 – Nominal airplane and optimized three-surface equivalent version.

	S_C m^2	x_{AC_C} m	x_{AC_W} m	λ_C	S_T m^2	E_{max}
Nominal	-	-	-2.21	-	2.35	20.04
Optimized	2.21	-0.061	-3.04	8.03	1.35	25.5

(reduced with respect to the nominal one, that was equal to $2.35\,m^2$). Surprisingly, the canard aspect ratio now is $\lambda_C = 8.033$, greater than the one obtained in the previous case. Rather than being an effect of the different elevator span ratios, we believe that this fact could indicate that the canard aspect ratio does not significantly influence the merit function.
For this optimal airplane, Fig. 5 shows the scheduling of the trim variables as functions of the lift coefficient.

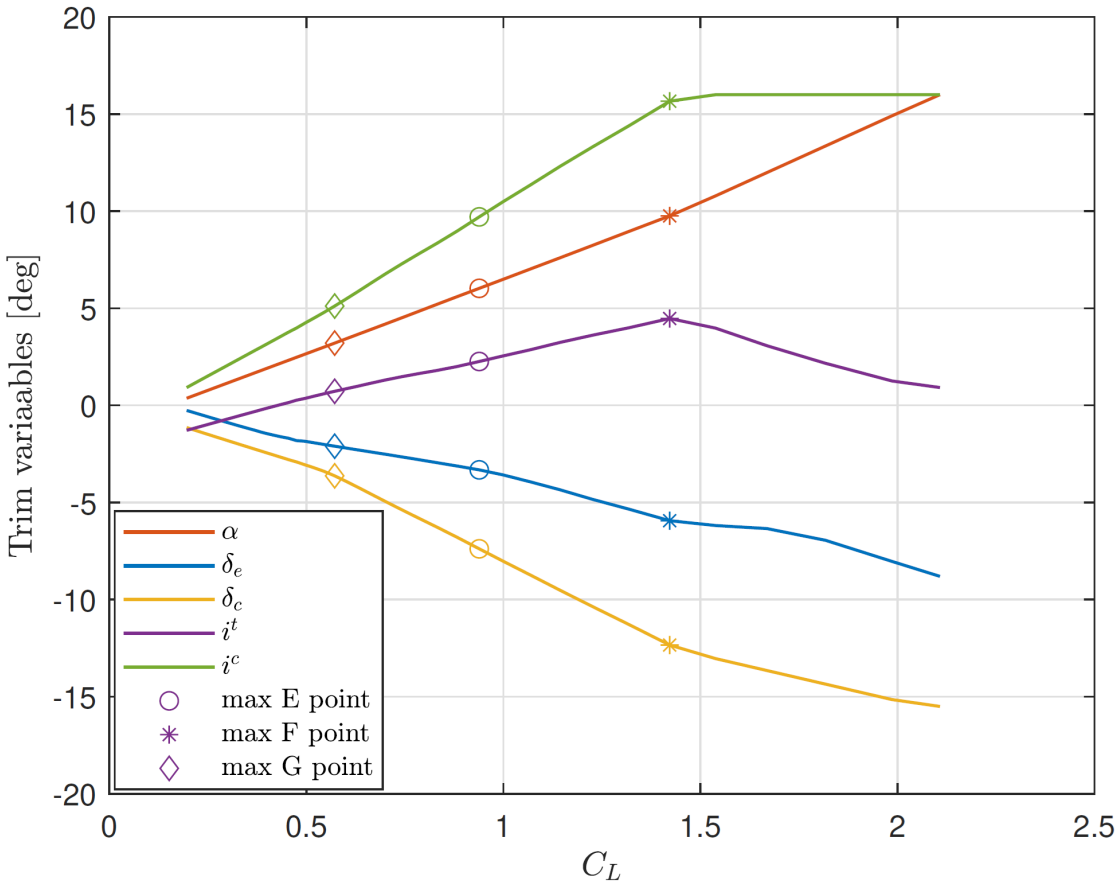

Figure 5 – Trim variable scheduling as a function of the lift coefficient

Finally, Fig. 6 shows the comparison between the nominal airplane and the two equivalent three-surface airplanes in terms of the lift-to-drag ratio. The solid thin blue curve refers to the nominal airplane, featuring $E_{max} = 20$ at $C_L = 0.75$ while the thick solid red and dashed green curves refer to the three-surface airplane respectively with nominal and halved elevator span ratio, b_{elev}/b_{tail}. The updated airplanes are characterized by higher maximum lift-to-drag ratios, which are reached at C_L of about 0.85, higher than the nominal case, indicating that the updated airplane will have lower optimal flight speeds. This however suggests that possible improvements could be obtained by reducing the wing area, a task that falls out of the scope of the present investigation.
Notice also that the three-surface airplanes have lower lift-to-drag ratios for C_L lower than 0.3. This is certainly expected: the addition of a new control surface penalizes the parasite drag of the overall airplane, jeopardizing the beneficial impact of the control redundancy and trim optimization. This could additionally indicate that the three-surface configuration with control redundancy may be less

effective for faster airplanes.

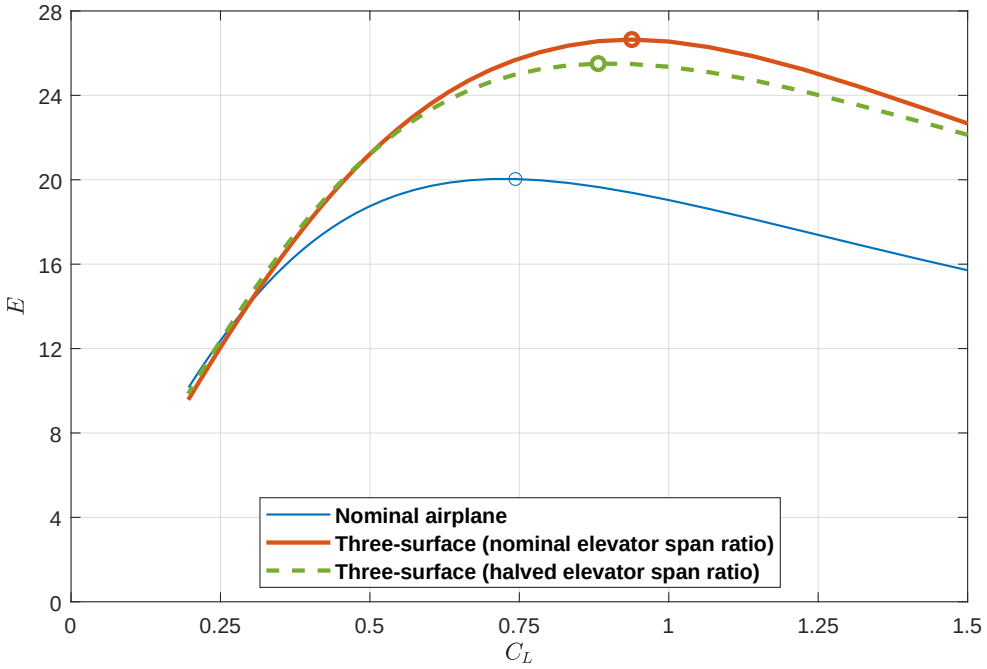

Figure 6 – Lift-to-drag ratios of the nominal and the three-surface updated airplanes as functions of lift coefficient C_L. Thin blue curve: nominal airplane; solid thick red curve: three-surface airplane with nominal elevator span ratio; dashed thick green line: three-surface airplane with halved elevator span ratio. Dots represent the maximum lift-to-drag for each configuration.

4. Conclusions

In this work, we presented a procedure to model, find the optimal trim, and design a three-surface airplane with redundant longitudinal control. The modeling is based on multiple estimation trials of the steady aerodynamic model through the Digital Datcom. The optimal trim, including the cancelation of the hinge moment, is based on the minimization of the drag coefficient for all airplane speeds. Finally, the preliminary design consists of two nested optimizations aimed at maximizing lift-to-drag ratio.
For a given three-surface geometry, the inner optimization loop aims at finding the schedule of the trim variables associated with the minimum drag and constrained to the satisfaction of both the longitudinal equilibrium and the cancellation of canard and elevator hinge moments.
The outer optimization loop, on the other hand, acts on some suitable geometry variables with the aim of turning an existing two-surface model into a three-surface one featuring a redundant control with improved lift-to-drag ratio performance.
From the analyses presented in this paper, we can derive the following conclusions.

- Although the semiempirical models included in Datcom do not consider the three-surface configurations, a suitable combination of multiple analyses can be used for modeling the steady aerodynamics of such airplanes.
- An additional degree of freedom in the longitudinal trim problem can be profitably exploited to maximize the aerodynamic performance of the trimmed polar, i.e. the relationship between lift and drag coefficients that incorporate the pitching moment equilibrium and the cancelation of hinge moments.
- A three-surface model with redundant longitudinal control equivalent to an existing two-surface one can be designed with an improved lift-to-drag ratio. In the analysis performed on a twin-engine propeller drive airplane loosely based on DA42, it was found a strong increase in the

maximum lift-to-drag ratio, quantified in about 30%, associated with the update of the traditional configuration into an equivalent three-surface one.

- The beneficial impact of the three-surface configuration with control redundancy seems effective, especially for relatively high lift coefficients. For low lift coefficients, the penalization due to the inclusion of a third surface in terms of parasite drag is not compensated by the improvements entailed by the trim optimization. This suggests that possibly faster airplanes may be less impacted by the proposed configuration updating.

Clearly, such promising results are only preliminary and the methodology should be consolidated. First, experimental data are needed to validate the estimation procedure of the aerodynamic model of the three-surface airplane. Secondarily, it should be understood whether the obtained increase in the aerodynamic performance is more due to the additional lifting surface or to the inclusion of a redundant longitudinal degree of freedom. The answer to this particular question may be useful for the preliminary design of such airplanes, a task that presents more critical points than the updating of an existing configuration faced in this paper.
All the aforementioned points are currently under investigation.

5. Contact Author Email Address

Corresponding author's contact: stefano.cacciola@polimi.it.

6. Copyright Statement

References

[1] Piaggio P180, Avanti Evo. Web page: http://www.avantievo.piaggioaerospace.it/. Last access: June 7, 2024.

[2] Strohmeyer D, Seubert R, Heinze W, Osterheld C and Fornasier L. Three surface aircraft —- a concept for future transport aircraft. *38th Aerospace Sciences Meeting and Exhibit*, pp 1–12, Reno, NV, USA, January 10–13, 2000. DOI: 10.2514/6.2000-566.

[3] Kendall E R. The theoretical minimum of induced drag of three-surface airplanes in trim. *Journal of Aircraft*. 1985, 22, 847—854. DOI: 10.2514/3.45214.

[4] Ricci S, Scotti A, and Zanotti D. Control of an all-movable foreplane for a three surface aircraft wind tunnel model. *Mechanical Systems and Signal Processing*, 2006, 20, 1044–1066. DOI: 10.1016/j.ymssp.2005.08.020.

[5] Agnew J, Hess J. Benefits of aerodynamic interaction to the three-surface configuration. *Journal of Aircraft*, 1980, 17, 823–827. DOI: 10.2514/3.57971.

[6] Cacciola S, Riboldi C E D and Arnoldi M. Three-surface model with redundant longitudinal control: Modeling, trim optimization and control in a preliminary design perspective. *Aerospace*, 2021, 8(5), 139. DOI: 10.3390/aerospace8050139.

[7] Pamadi B N. *Performance, Stability, Dynamics and Control of Aircraft*, American Institute of Aeronautics and Astronautics: Reston, VA, USA, 1998.

[8] Levy D. Prediction of average downwash gradient for canard configurations. In Proceedings of the 30th AIAA Aerospace Science Meeting and Exhibit, Reno, NV, USA, January 6–9, 1992. DOI: 10.2514/6.1992-284.

[9] Riboldi C E D, Cacciola S and Ceffa L. Studying and Optimizing the Take-Off Performance of Three-Surface Aircraft, *Aerospace* 2022, 9(3), 139. https://doi.org/10.3390/aerospace9030139.

[10] Fink R D. USAF Stability and Control Datcom, AFWAL-TR-83-3048, Flight Dynamics Laboratories (AFWAL/FIGC), Air Force Wright Aeronautical Laboratories, Wrigth–Patterson Air Force Base, Ohio 4543, April 1978.

[11] Roskam J. *Airplane Design*. Roskam Aviation and Engineering Corporation: Ottawa, KS, USA, 1988.

[12] Byrd R H, Gilbert J C and Nocedal J. A Trust Region Method Based on Interior Point Techniques for Nonlinear Programming. *Mathematical Programming*, 2000, 89(1), 149—185. DOI: 10.1007/s101070000189.